The Star Formation Newsletter

A community newsletter on Star and Planet Formation research

No. 360 — 31 December 2022

Editor: João Alves www.starformation.news

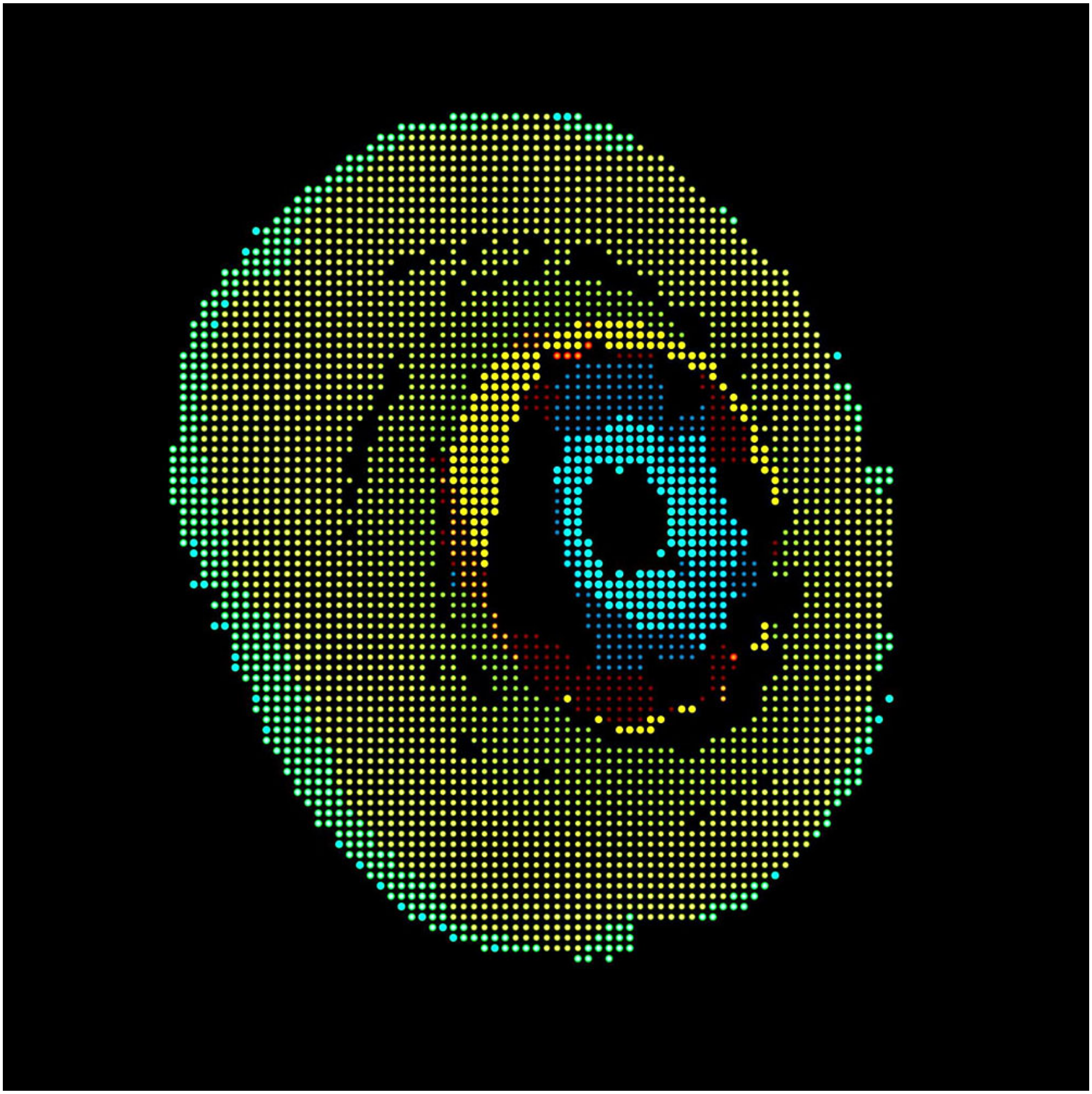

Links to sections

Interviews	Reviews	Perspective	Favorite objects	Archive
Meetings	Jobs	New PhDs	Announcements	Books

Cover image caption

Artstics impression of EX Lupi by Ruth Jarman and Joe Gerhardt (Semiconductor). This image is part of **Spectral Constellations** a series of generative animations, driven by scientific data of young stars. Credits: Semiconductor. Spectral Constellations was commissioned through a residency with the **Planet Disk Connection group**, STFC, and DJCAD at the University of Dundee, Scotland.

Note from the Editor

The Star Formation Newsletter is now on the web at **www.starformation.news**. This PDF file contains the monthly Abstracts and links to the different Newsletter sections. Red text in this PDF is a url link. Submitting an abstract to the SFN is as simple as entering the arXiv ID (e.g., 2006.10139) in a web form on the SFN web site. **Do not remove the LaTeX formatting when submitting to the arXiv**. If you do, your abstract will not look great either at the arXiv or the SFN.

Abstracts

1. Discovery of interstellar NC4NH+: dicyanopolyynes are indeed abundant in space

M. Agundez, C. Cabezas, N. Marcelino, R. Fuentetaja, B. Tercero, P. de Vicente, J. Cernicharo ★ The previous detection of two species related to the non polar molecule cyanogen (NCCN), its protonated form (NCCNH+) and one metastable isomer (CNCN), in cold dense clouds supported the hypothesis that dicyanopolyynes are abundant in space. Here we report the first identification in space of NC4NH+, which is the protonated form of NC4N, the second member of the series of dicyanopolyynes after NCCN. The detection was based on the observation of six harmonically related lines within the Yebes 40m line survey of TMC-1 QUIJOTE. The six lines can be fitted to a rotational constant B = 1293.90840 +/- 0.00060 MHz and a centrifugal distortion constant D = 28.59 +/- 1.21 Hz. We confidently assign this series of lines to NC4NH+ based on high-level ab initio calculations, which supports the previous identification of HC5NH+ by Marcelino et al. (2020) from the observation of a series of lines with a rotational constant 2 MHz lower than that derived here. The column density of NC4NH+ in TMC-1 is (1.1 +1.4 -0.6)e10 cm-2, which implies that NC4NH+ is eight times less abundant than NCCNH+. The species CNCN, previously reported toward L483 and tentatively in TMC-1, is confirmed in this latter source. We estimate that NCCN and NC4N are present in TMC-1 with abundances a few times to one order of magnitude lower than HC3N and HC5N, respectively. This means that dicyanopolyynes NC-(CC)n-CN are present at a lower level than the corresponding monocyanopolyynes HCC-(CC)n-CN. The reactions of the radicals CN and C3N with HNC arise as the most likely formation pathways to NCCN and NC4N in cold dense clouds.

2. On the Number of Stars in the Sun's Birth Cluster

Sota Arakawa, Eiichiro Kokubo ★ The Sun is thought to be formed within a star cluster. The coexistence of ^{26}Al-rich and ^{26}Al-poor calcium–aluminum-rich inclusions indicates that a direct injection of ^{26}Al-rich materials from a nearby core-collapse supernova should occur in the first 10^5 years of the solar system. Therefore, at least one core-collapse supernova should occur within the duration of star formation in the Sun's birth cluster. Here we revisit the number of stars in the Sun's birth cluster from the point of view of the probability for acquiring at least one core-collapse supernova within the finite duration of star formation in the birth cluster. We find that the number of stars in the birth cluster can be significantly larger than that previously considered, depending on the duration of star formation.

3. Time-dependent Monte Carlo continuum radiative transfer

A. Bensberg, S. Wolf ★ Aims. We present an implementation of an algorithm for 3D time-dependent Monte Carlo radiative transfer. It allows one to simulate temperature distributions as well as images and spectral energy distributions of the scattered light and thermal reemission radiation for variable illuminating and heating sources embedded in dust distributions, such as circumstellar disks and dust shells on time scales up to weeks. Methods. We extended the publicly available 3D Monte Carlo radiative transfer code POLARIS with efficient methods for the simulation of temperature distributions, scattering, and thermal reemission of dust distributions illuminated by temporally variable radiation sources. The influence of the chosen temporal step width and the number of photon packages per time step as key parameters for a given configuration is shown by simulating the temperature distribution in a spherical envelope around an embedded central star. The effect of the optical depth on the temperature simulation is discussed for the spherical envelope as well as for a model of a circumstellar disk with an embedded star. Finally, we present simulations of an outburst of a star surrounded by a circumstellar disk. Results. The presented algorithm for time-dependent 3D continuum Monte Carlo radiative transfer is a valuable basis for preparatory studies as well as for the analysis of continuum observations of the dusty environment around variable sources, such as accreting young stellar objects. In particular, the combined study of light echos in the optical and near-infrared wavelength range and the corresponding time-dependent thermal reemission observables of variable, for example outbursting sources, becomes possible on all involved spatial scales.

4. Chemical modeling of Orion Nebula Cluster disks: evidence for massive, compact gas disks with ISM-like gas-to-dust ratios

Ryan D. Boyden, Josh A. Eisner ★ The stellar cluster environment is expected to play a central role in the evolution of circumstellar disks. We use thermochemical modeling to constrain the dust and gas masses, disk sizes, UV and X-ray radiation fields, viewing geometries, and central stellar masses of 20 Class II disks in the Orion Nebula Cluster (ONC). We fit a large grid of disk models to 350 GHz continuum, CO $J = 3-2$, and HCO^+ $J = 4-3$ ALMA observations of each target, and we introduce a procedure for modeling interferometric observations of gas disks detected in absorption against a bright molecular cloud background. We find that the ONC disks are massive and compact, with typical radii < 100 AU, gas masses $\geq 10^{-3}$ $M_\odot$, and gas-to-dust ratios ≥ 100. The ISM-like gas-to-dust ratios derived from our modeling suggest that compact, externally-irradiated disks in the ONC are less prone to gas-phase CO depletion than the massive and extended gas disks that are commonly found in nearby low-mass star-forming regions. The presence of massive gas disks indicates that external photoevaporation may have only recently begun operating in the ONC, though it remains unclear whether other cluster members are older and more evaporated than the ones in our sample. Finally, we compare our dynamically-derived stellar masses with the stellar masses predicted from evolutionary models and find excellent agreement. Our study has significantly increased the number of dynamical mass measurements in the mass range ≤ 0.5 $M_\odot$, demonstrating that the ONC is an ideal region for obtaining large samples of dynamical mass measurements towards low-mass M-dwarfs.

5. The Star Formation History of the Milky Way's Nuclear Star Cluster

Zhuo Chen, Tuan Do, Andrea M. Ghez, Matthew Hosek Jr., Anja Feldmeier-Krause, Devin Chu, Rory Bentley, Jessica R. Lu, Mark R. Morris ★ We report the first star formation history study of the Milky Way's nuclear star cluster (NSC) that includes observational constraints from a large sample of stellar metallicity measurements. These metallicity measurements were obtained from recent surveys from Gemini and VLT of 770 late-type stars within the central 1.5 pc. These metallicity measurements, along with photometry and spectroscopically derived temperatures, are forward modeled with a Bayesian inference approach. Including metallicity measurements improves the overall fit quality, as the low-temperature red giants that were previously difficult to constrain are now accounted for, and the best fit favors a two-component model. The dominant component contains 93($\overline{[M/H]}$ ~0.45), and has an age of 5^{+3}_{-2} Gyr, which is ~3 Gyr younger than earlier studies with fixed (solar) metallicity; this younger age challenges co-evolutionary models in which the NSC and supermassive black holes formed simultaneously at early times. The minor population component has low metallicity ($\overline{[M/H]}$ ~ -1.1) and contains ~7- 5 Gyr old). Using the estimated parameters, we infer the following NSC stellar remnant population (with ~18neutron stars, 2.5×10^5 stellar mass black holes (BHs) and 2.2×10^4 BH-BH binaries. These predictions result in 2-4 times fewer neutron stars compared to earlier predictions that assume solar metallicity, introducing a possible new path to understand the so-called "missing pulsar problem". Finally, we present updated predictions for the BH-BH merger rates (0.01-3 $Gpc^{-3}yr^{-1}$).

6. The JCMT BISTRO-2 Survey: Magnetic Fields of the Massive DR21 Filament

Tao-Chung Ching and the BISTRO team ★ We present 850 μm dust polarization observations of the massive DR21 filament from the B-fields In STar-forming Region Observations (BISTRO) survey, using the POL-2 polarimeter and the SCUBA-2 camera on the James Clerk Maxwell Telescope. We detect ordered magnetic fields perpendicular to the parsec-scale ridge of the DR21 main filament. In the sub-filaments, the magnetic fields are mainly parallel to the filamentary structures and smoothly connect to the magnetic fields of the main filament. We compare the POL-2 and Planck dust polarization observations to study the magnetic field structures of the DR21 filament on 0.1–10 pc scales. The magnetic fields revealed in the Planck data are well aligned with those of the POL-2 data, indicating a smooth variation of magnetic fields from large to small scales. The plane-of-sky magnetic field strengths derived from angular dispersion functions of dust polarization are 0.6–1.0 mG in the DR21 filament and $\sim$ 0.1 mG in the surrounding ambient gas. The mass-to-flux ratios are found to be magnetically supercritical in the filament and slightly subcritical to nearly critical in the ambient gas. The alignment between column density structures and magnetic fields changes from random alignment in the low-density ambient gas probed by Planck to mostly perpendicular in the high-density main filament probed by JCMT. The magnetic field structures of the DR21 filament are in agreement with MHD simulations of a strongly magnetized medium, suggesting that magnetic fields play an important role in shaping the DR21 main filament and sub-filaments.

7. Making the Solar System

John Chambers ★ We model the early stages of planet formation in the Solar System, including continual planetesimal formation, and planetesimal and pebble accretion onto planetary embryos in an evolving disk driven by a disk wind. The aim is to constrain aspects of planet formation that have large uncertainties by matching key characteristics of the Solar System. The model produces a good fit to these characteristics for a narrow range of parameter space. Planetary growth beyond the ice line is dominated by pebble accretion. Planetesimal accretion is more important inside the ice line. Pebble accretion inside the ice line is slowed by higher temperatures, partial removal of inflowing pebbles by planetesimal formation and pebble accretion further out in the disk, and increased radial velocities due to gas advection. The terrestrial planets are prevented from accreting much water ice because embryos beyond the ice line reach the pebble isolation mass before the ice line enters the terrestrial-planet region. When only pebble accretion is considered, embryos typically remain near their initial mass or grow to the pebble-isolation mass. Adding planetesimal accretion allows Mars-sized objects to form inside the ice line, and allows giant-planet cores to form over a wider region beyond the ice line. In the region occupied by Mercury, pebble Stokes numbers are small. This delays the formation of embryos and stunts their growth, so that only low-mass planets can form here.

8. UV-driven Chemistry as a Signpost for Late-stage Planet Formation

Jenny K. Calahan, Edwin A. Bergin, Arthur D. Bosman, Evan Rich, Sean M. Andrews, Jennifer B. Bergner, L. Ilsedore Cleeves, Viviana V. Guzman, Jane Huang, John D. Ilee, Charles J. Law, Romane Le Gal, Karin I. Oberg, Richard Teague, Catherine Walsh, David J. Wilner, Ke Zhang ★ The chemical reservoir within protoplanetary disks has a direct impact on planetary compositions and the potential for life. A long-lived carbon-and nitrogen-rich chemistry at cold temperatures ($<=$50K) is observed within cold and evolved planet-forming disks. This is evidenced by bright emission from small organic radicals in 1-10 Myr aged systems that would otherwise have frozen out onto grains within 1 Myr. We explain how the chemistry of a planet-forming disk evolves from a cosmic-ray/X-ray-dominated regime to an ultraviolet-dominated chemical equilibrium. This, in turn, will bring about a temporal transition in the chemical reservoir from which planets will accrete. This photochemical dominated gas phase chemistry develops as dust evolves via growth, settling and drift, and the small grain population is depleted from the disk atmosphere. A higher gas-to-dust mass ratio allows for deeper penetration of ultraviolet photons is coupled with a carbon-rich gas (C/O $>$ 1) to form carbon-bearing radicals and ions. This further results in gas phase formation of organic molecules, which then would be accreted by any actively forming planets present in the evolved disk.

9. Length-scales and Dynamics of Carina's Western Wall

Turlough Downes, Patrick Hartigan, Andrea Isella ★ We present a variety of analyses of the turbulent dynamics of the boundary of a photo-dissociation region (PDR) in the Carina Nebula using high resolution ALMA observations. Using Principal Component Analysis we suggest that the turbulence in this molecular cloud is driven at large scales. Analysis of the centroid velocity structure functions indicate that the turbulence is dominated by shocks rather than local (in k-space) transport of energy. We further find that length-scales in the range 0.02 - 0.03 pc are important in the dynamics of this cloud and this finding is supported by analysis of the dominant emission structure length-scale. These length-scales are well resolved by the observational data and we conclude that the apparent importance of this range of scales is physical in origin. Given that it is also well within the range strongly influenced by ambipolar diffusion, we conclude that it is not primarily a product of turbulence alone, but is more likely to be a result of the interplay between gravity and turbulence. Finally, through comparison of these results with previous observations of H2 emission from the Western Wall we demonstrate that observations of a PDR can be used to probe the internal structure of the undisturbed portion of a molecular cloud.

10. Discovery of a New Molecular Bubble-Outflow Structure in the Taurus B18 Cloud

Yan Duan, Di Li, Paul F. Goldsmith, Laurent Pagani, Tao-Chung Ching, Shu Liu, Jinjin Xie, Chen Wang ★ Star formation can produce bubbles and outflows, as a result of stellar feedback. Outflows and bubbles inject momentum and energy into the surrounding interstellar medium, and so are related to the overall energy balance of the molecular cloud. Molecular bubbles can be resolved by higher-resolution radio telescopes to quantify the effect of star formation on molecular clouds. We report here the identification of a new molecular bubble with an outflow, and an Herbig Haro object, HH319, located at the bubble center. Multi-wavelength data have been utilized to study its spatial structure, energy injection, and dynamical timescale. This bubble has a kinetic energy of 5.8×10^{43} erg within the smallest radius of a bubble in Taurus, 0.077 pc. The bubble formed ~70,000 years ago. According to the proper motion velocities of protostars from *Gaia* EDR3, the T Tauri binary stars (FY Tau and FZ Tau) at the southwest edge of the bubble may have produced the outflow-bubble structure. This is an unusual new structure found in low- and intermediate-mass star formation regions. Only a bubble in Orion A, driven by V380 Ori, has a similar structure. The bubble-outflow structure provides additional observational evidence for the theory of stellar wind from T Tauri stars. It enhances our understanding of how stellar feedback acts on molecular clouds.

11. Constraining the turbulence and the dust disk in IM Lup: onset of planetesimal formation

Riccardo Franceschi, Tilman Birnstiel, Thomas Henning, Anirudh Sharma ★ Observations of protoplanetary disks provide information on planet formation and the reasons for the diversity of planetary systems. The key to understanding planet formation is the study of dust evolution from small grains to pebbles. Smaller grains are well-coupled to the gas dynamics, and their distribution is significantly extended above the disk midplane. Larger grains settle much faster and are efficiently formed only in the midplane. By combining near-infrared polarized light and millimeter observations, it is possible to constrain the spatial distribution of both the small and large grains. We aim to construct detailed models of the size distribution and vertical/radial structure of the dust particles in protoplanetary disks based on observational data. In particular, we are interested in recovering the dust distribution in the IM Lup protoplanetary disk. We create a physical model for the dust distribution of protoplanetary disks and simulate the radiative transfer of the millimeter continuum and the near-infrared polarized radiation. Using a Markov chain Monte Carlo method, we compare the derived images to the observations available for the IM Lup disk to constrain the best physical model for IM Lup and to recover the vertical grain size distribution. The millimeter and near-infrared emission tightly constrain the dust mass and grain size distribution of our model. We find size segregation in the dust distribution, with millimeter-sized grains in the disk midplane. These grains are efficiently formed in the disk, possibly by sedimentation-driven coagulation, in accord with the short settling timescales predicted by our model. This also suggests a high dust-to-gas ratio at smaller radii in the midplane, possibly triggering streaming instabilities and planetesimal formation in the inner disk.

12. A 3D View of Orion: I. Barnard's Loop

Michael M. Foley, Alyssa Goodman, Catherine Zucker, John C. Forbes, Ralf Konietzka, Cameren Swiggum, João Alves, John Bally, Juan D. Soler, Josefa E. Großschedl, Shmuel Bialy, Michael Y. Grudić, Reimar Leike, Torsten Ensslin ★ Barnard's Loop is a famous arc of Hα emission located in the Orion star-forming region. Here, we provide evidence of a possible formation mechanism for Barnard's Loop and compare our results with recent work suggesting a major feedback event occurred in the region around 6 Myr ago. We present a 3D model of the large-scale Orion region, indicating coherent, radial, 3D expansion of the OBP-Near/Briceño-1 (OBP-B1) cluster in the middle of a large dust cavity. The large-scale gas in the region also appears to be expanding from a central point, originally proposed to be Orion X. OBP-B1 appears to serve as another possible center, and we evaluate whether Orion X or OBP-B1 is more likely to be the cause of the expansion. We find that neither cluster served as the single expansion center, but rather a combination of feedback from both likely propelled the expansion. Recent 3D dust maps are used to characterize the 3D topology of the entire region, which shows Barnard's Loop's correspondence with a large dust cavity around the OPB-B1 cluster. The molecular clouds Orion A, Orion B, and Orion λ reside on the shell of this cavity. Simple estimates of gravitational effects from both stars and gas indicate that the expansion of this asymmetric cavity likely induced anisotropy in the kinematics of OBP-B1. We conclude that feedback from OBP-B1 has affected the structure of the Orion A, Orion B, and Orion λ molecular clouds and may have played a major role in the formation of Barnard's Loop.

13. Two saturated states of the vertical shear instability in protoplanetary disks with vertically varying cooling times

Yuya Fukuhara, Satoshi Okuzumi, Tomohiro Ono ★ Turbulence in protoplanetary disks plays an important role in dust evolution and planetesimal formation. The vertical shear instability (VSI) is one of the candidate hydrodynamic mechanisms that can generate turbulence in the outer disk regions. The VSI requires rapid gas cooling in addition to vertical shear. A linear stability analysis suggests that the VSI may not operate around the midplane where gas cooling is inefficient. In this study, we investigate the nonlinear outcome of the VSI in disks with a linearly VSI-stable midplane region. We perform two-dimensional global hydrodynamical simulations of an axisymmetric disk with vertically varying cooling times. The vertical cooling time profile determines the thicknesses of the linearly VSI-stable midplane layer and unstable layers above and below the midplane. We find that the thickness of the midplane stable layer determines the vertical structure of VSI-driven turbulence in the nonlinear saturated state. We identify two types of final saturated state: (1) T states characterized by vertical turbulent motion penetrating into the VSI-stable midplane layer and (2) pT states characterized by turbulent motion confined in the unstable layers. The pT states are realized when the midplane VSI-stable layer is thicker than two gas scale heights. We also find that the VSI-driven turbulence is largely suppressed at all heights when the VSI-unstable region lying above and below the midplane is thinner than two gas scale heights. We present empirical formulas that predict the strength of VSI-driven turbulence as a function of the thicknesses of the unstable and stable layers. These formulas will be useful for studying how VSI-driven turbulence and dust grains controlling the disk cooling efficiency evolve simultaneously.

14. Distance determination of molecular clouds in the 1st quadrant of the Galactic plane using deep learning : I. Method and Results

Shinji Fujita, A. M. Ito, Yusuke Miyamoto, Yasutomo Kawanishi, Kazufumi Torii, Yoshito Shimajiri, Atsushi Nishimura, Kazuki Tokuda, Toshikazu Ohnishi, Hiroyuki Kaneko, Tsuyoshi Inoue, Shunya Takekawa, Mikito Kohno, Shota Ueda, Shimpei Nishimoto, Ryuki Yoneda, Kaoru Nishikawa, Daisuke Yoshida ★ Machine learning has been successfully applied in varied field but whether it is a viable tool for determining the distance to molecular clouds in the Galaxy is an open question. In the Galaxy, the kinematic distance is commonly employed as the distance to a molecular cloud. However, there is a problem in that for the inner Galaxy, two different solutions, the "Near" solution, and the "Far" solution, can be derived simultaneously. We attempted to construct a two-class ("Near" or "Far") inference model using a Convolutional Neural Network (CNN), a form of deep learning that can capture spatial features generally. In this study, we used the CO dataset toward the 1st quadrant of the Galactic plane obtained with the Nobeyama 45-m radio telescope (l = 62-10 degree, $|b| < 1$ degree). In the model, we applied the three-dimensional distribution (position-position-velocity) of the 12CO (J=1-0) emissions as the main input. The dataset with "Near" or "Far" annotation was made from the HII region catalog of the infrared astronomy satellite WISE to train the model. As a result, we could construct a CNN model with a 76training dataset. By using the model, we determined the distance to molecular clouds identified by the CLUMPFIND algorithm. We found that the mass of the molecular clouds with a distance of < 8.15 kpc identified in the 12CO data follows a power-law distribution with an index of about -2.3 in the mass range of M $>10^3$ Msun. Also, the detailed molecular gas distribution of the Galaxy as seen from the Galactic North pole was determined.

15. Clustered Formation of Massive Stars within an Ionized Rotating Disk

Roberto Galván-Madrid, Qizhou Zhang, Andrés Izquierdo, Charles J. Law, Thomas Peters, Eric Keto, Hauyu Baobab Liu, Paul T. P. Ho, Adam Ginsburg, Carlos Carrasco-González ★ We present ALMA observations with a 800 au resolution and radiative-transfer modelling of the inner part ($r \approx 6000$ au) of the ionized accretion flow around a compact star cluster in formation at the center of the luminous ultra-compact (UC) HII region G10.6-0.4. We modeled the flow with an ionized Keplerian disk with and without radial motions in its outer part, or with an external Ulrich envelope. The MCMC fits to the data give total stellar masses $M_\star$ from 120 to 200 $M_\odot$, with much smaller ionized-gas masses $M_{\mathrm{ion-gas}} = 0.2$ to 0.25 $M_\odot$. The stellar mass is distributed within the gravitational radius $R_g \approx 1000$ to 1500 au, where the ionized gas is bound. The viewing inclination angle from the face-on orientation is $i = 49$ to 56 deg. Radial motions at radii $r > R_g$ converge to $v_{r,0} \approx 8.7$ km/s, or about the speed of sound of ionized gas, indicating that this gas is marginally unbound at most. From additional constraints on the ionizing-photon rate and far-IR luminosity of the region, we conclude that the stellar cluster consists of a few massive stars with $M_{\mathrm{star}} = 32$ to 60 $M_\odot$, or one star in this range of masses accompanied by a population of lower-mass stars. Any active accretion of ionized gas onto the massive (proto)stars is residual. The inferred cluster density is very large, comparable to that reported at similar scales in the Galactic Center. Stellar interactions are likely to occur within the next Myr.

16. Relation between metallicities and spectral energy distributions of Herbig Ae/Be stars. A potential link with planet formation

J. Guzman-Diaz, B. Montesinos, I. Mendigutia, M. Kama, G. Meeus, M. Vioque, R. D. Oudmaijer, E. Villaver ★ (Abridged) The stellar metallicity, [M/H], may have important implications for planet formation. In particular, Kama et al. proposed that the deficit of refractory elements in the surfaces of some Herbig Ae/Be stars (HAeBes) may be linked to the presence of disk cavities likely caused by Jovian planets that trap the metal-rich content. This work aims to provide a robust test on the previous proposal by analyzing the largest sample of HAeBes with homogeneously derived [M/H] values, stellar, and circumstellar properties. [M/H] values of 67 HAeBes were derived based on observed spectra and Kurucz synthetic models. Statistical analyses were carried out aiming to test the potential relation between [M/H] and the group I sources from the spectral energy distribution (SED) classification by Meeus et al., associated to the presence of cavities potentially carved by giant planets. Our study robustly confirms that group I sources tend to have a lower [M/H] than that of group II HAeBes. A similar analysis involving SED-based transitional disks does not reveal such a relation, indicating that not all processes capable of creating dust holes have an effect on the stellar abundances. We also show that the observed [M/H] differences are not driven by environmental effects. Finally, group I sources tend to have stronger (sub-) mm continuum emission presumably related to the presence of giant planets. Indeed, literature results indicate that disk substructures probably associated to their presence are up to ten times more frequent in group I HAeBes. We provide indirect evidences suggesting that giant planets are more frequent around group I/low [M/H] stars than around the rest of the HAeBes. However, the direct test requires multiple detections of forming planets in their disks, so far limited to the candidate around the metal depleted ([M/H] = -0.35 +- 0.25) group I HAeBe star AB Aur.

17. Models of Rotating Infall for the B335 Protostar

Neal J. Evans II, Yao-Lun Yang, Joel D. Green, Bo Zhao, James Di Francesco, Jeong-Eun Lee, Jes K. Jørgensen, Minho Choi, Philip C. Myers, Diego Mardones ★ Models of the protostellar source, B335, are developed using axisymmetric three-dimensional models to resolve conflicts found in one-dimensional models. The models are constrained by a large number of observations, including ALMA, Herschel, and Spitzer data. Observations of the protostellar source B335 with ALMA show red-shifted absorption against a central continuum source indicative of infall in the HCO^+ and HCN $J = 4 \rightarrow 3$ transitions. The data are combined with a new estimate of the distance to provide strong constraints to three-dimensional radiative transfer models including a rotating, infalling envelope, outflow cavities, and a very small disk. The models favor ages since the initiation of collapse between 3×10^4 and 4×10^4 yr for both the continuum and the lines, resolving a conflict found in one-dimensional models. The models under-predict the continuum emission seen by ALMA, suggesting an additional component such as a pseudo-disk. The best-fitting model is used to convert variations in the 4.5 μm flux in recent years into a model for a variation of a factor of 5-7 in luminosity over the last 8 years.

18. X-Shooter Survey of Young Intermediate Mass Stars – I. Stellar Characterization and Disc Evolution

Daniela P. Iglesias, Olja Panić, Mario van den Ancker, Monika G. Petr-Gotzens, Lionel Siess, Miguel Vioque, Ilaria Pascucci, René Oudmaijer, James Miley ★ Intermediate mass stars (IMSs) represent the link between low-mass and high-mass stars and cover a key mass range for giant planet formation. In this paper, we present a spectroscopic survey of 241 young IMS candidates with IR-excess, the most complete unbiased sample to date within 300 pc. We combined VLT/X-Shooter spectra with BVR photometric observations and Gaia DR3 distances to estimate fundamental stellar parameters such as Teff, mass, radius, age, and luminosity. We further selected those stars within the intermediate mass range 1.5 <= Mstar/Msun <= 3.5 and discarded old contaminants. We used 2MASS and WISE photometry to study the IR-excesses of the sample, finding 92 previously unidentified stars with IR-excess. We classified this sample into 'protoplanetary', 'hybrid candidates' and 'debris' discs based on their observed fractional excess at 12microns, finding a new population of 17 hybrid disc candidates. We studied inner disc dispersal timescales for $\lambda < 10\mu$m and found very different trends for IMSs and low mass stars (LMSs). IMSs show excesses dropping fast during the first 6 Myrs independently of the wavelength, while LMSs show consistently lower fractions of excess at the shortest wavelengths and increasingly higher fractions for longer wavelengths, with slower dispersal rates. In conclusion, this study demonstrates empirically that IMSs dissipate their inner discs very differently than LMSs, providing a possible explanation for the lack of short period planets around IMSs.

19. Dust Motion and Possibility of Dust Growth in a Growing Circumstellar Disk

Shunta Koga, Masahiro N. Machida ★ We calculate the evolution of a star-forming cloud core using a three-dimensional resistive magnetohydrodynamics simulation, treating dust grains as Lagrangian particles, to investigate the dust motion in the early star formation stage. We prepare six different-sized set of dust particles in the range $a_{\rm d} = 0.01$–$1000\,\mu$m, where $a_{\rm d}$ is the dust grain size. In a gravitationally collapsing cloud, a circumstellar disk forms around a protostar and drives a protostellar outflow. Almost all the small dust grains ($a_{\rm d} \lesssim 10$–$100\,\mu$m) initially distributed in the region $\theta_0 \lesssim 45°$ are ejected from the center by the outflow, where θ_0 is the initial zenith angle relative to the rotation axis, whereas only a small number of the large dust grains ($a_{\rm d} \gtrsim 100\,\mu$m) distributed in the region are ejected. All other grains fall onto either the protostar or disk without being ejected by the outflow. Regardless of the dust grain size, the behavior of the dust motion is divided into two trends after dust particles settle into the circumstellar disk. The dust grains reaching the inner disk region from the upper envelope preferentially fall onto the protostar, while those reaching the outer disk region or disk outer edge from the envelope can survive without an inward radial drift. These surviving grains can induce dust growth. Thus, we expect that the outer disk regions could be a favored place of planet formation.

20. The shocked molecular layer in RCW 120

M. S. Kirsanova, Ya. N. Pavlyuchenkov, A. O. H. Olofsson, D. A. Semenov, A. F. Punanova ★ Expansion of wind-blown bubbles or HII regions lead to formation of shocks in the interstellar medium, which compress surrounding gas into dense layers. We made spatially and velocity-resolved observations of the RCW 120 PDR and nearby molecular gas with CO(6-5) and 13CO(6-5) lines and distinguished a bright CO-emitting layer, which we related with the dense shocked molecular gas moving away from the ionizing star due to expansion of HII region. Simulating gas density and temperature, as well as brightness of several CO and C+ emission lines from the PDR, we found reasonable agreement with the observed values. Analysing gas kinematics, we revealed the large-scale shocked PDR and also several dense environments of embedded protostars and outflows. We observe the shocked layer as the most regular structure in the CO(6-5) map and in the velocity space, when the gas around YSOs is dispersed by the outflows.

21. The molecular environment of the solar-type protostar IRAS 16293-2422

K. Angelique Kahle, Antonio Hernández-Gómez, Friedrich Wyrowski, Karl M. Menten ★ Studying the physical and chemical processes leading to the formation of low-mass stars is crucial for understanding the origin of our Sun and the Solar System. In particular, analyzing the emission and absorption lines from molecules is a fundamental tool to obtain information on the kinematics and chemistry at the very early stages of star formation. In this work we aim to examine the spatial structures and molecular abundances of material surrounding the very well-known low-mass binary protostar IRAS 16293-2422 and the prestellar core 16293E, which are embedded in the Lynds 1689N dark cloud. We have used the LAsMA heterodyne array installed on the Atacama Pathfinder EXperiment (APEX) 12 meter submillimeter telescope to image a region of about 0.12x0.12pc^2 around IRAS 16293-2422 and 16293E and to study their molecular environment covering 45.6GHz in a frequency range from 277GHz to 375GHz. We have identified 144 transitions from 36 molecular species, including isotopologues. The maps reveal the envelope to have a complex morphology around the cloud cores and the emission peaks known as E1, E2, W1, W2, and HE2, including the outflow structure arising from IRAS 16293-2422. Using several transitions of para-H_2CO, we have derived new lower limits for the kinetic temperatures toward IRAS 16293-2422 and the surrounding emission peaks. Based on these temperatures, H_2 volume densities and column densities for all detected species were derived around the cloud cores and all emission peaks. Our new observations further confirm the scenario of an outflow arising from IRAS 16293-2422 interacting with the prestellar core 16293E. We observe a large-scale velocity gradient across the molecular cloud. Furthermore, we see clear chemical differences at the examined positions. The data suggests that emission peak W2 may be related to a colder dust source.

22. Disk dissipation, giant planet formation and star-formation-rate fluctuations in the past three-million-year history of Gould's Belt

Mingchao Liu, Jinhua He, Jixing Ge, Tie Liu, Yuping Tang, Xuzhi Li ★ Although episodic star formation (SF) had been suggested for nearby SF regions, a panoramic view to the latest episodic SF history in the solar neighborhood is still missing. By uniformly constraining the slope α of infrared spectral energy distributions (SEDs) of young stellar objects (YSOs) in the 13 largest Gould's Belt (GB) protoclusters surveyed by Spitzer Space Telescope, we have constructed a cluster-averaged histogram of α representing YSO evolution lifetime as a function of the α value. Complementary to the traditional SED classification scheme (0, I, F, II, III) that is based on different α values, a staging scheme (A,B,C,D,E) of SED evolution is advised on the basis of the α statistical features that can be better matched to the physical stages of disk dissipation and giant planet formation. This has also allowed us to unravel the fluctuations of star formation rate (SFR) in the past three-million-year (3 Myr) history of these GB protoclusters. Diverse evolutionary patterns such as single peak, double peaks and on-going acceleration of SFR are revealed. The SFR fluctuations are between 20% $\sim$ 60% ($\sim$ 40% on average) and no dependence on the average SFR or the number of SFR episodes is found. However, spatially close protoclusters tend to share similar SFR fluctuation trends, indicating that the driving force of the fluctuations should be at size scales beyond the typical cluster sizes of several parsec.

23. Dust Rings and Cavities in the Protoplanetary Disks around HD 163296 and DoAr 44

Harrison Leiendecker, Hannah Jang-Condell, Neal J. Turner, Adam D. Myers ★ We model substructure in the protoplanetary disks around DoAr 44 and HD 163296 in order to better understand the conditions under which planets may form. We match archival millimeter-wavelength thermal emission against models of the disks' structure that are in radiation balance with the starlight heating and in vertical hydrostatic equilibrium, and then compare to archival polarized scattered near-infrared images of the disks. The millimeter emission arises in the interior, while the scattered near-infrared radiation probes the disks' outer layers. Our best model of the HD 163296 disk has dust masses 81 ± 13 $M_\oplus$ in the inner ring at 68 au and 82^{+26}_{-16} $M_\oplus$ in the outer ring at 102 au, both falling within the range of estimates from previous studies. Our DoAr 44 model has total dust mass $84^{+7.0}_{-3.5}$ $M_\oplus$. Unlike HD 163296, DoAr 44 as of yet has no detected planets. If the central cavity in the DoAr 44 disk is caused by a planet, the planet's mass must be at least 0.5 M_J and is unlikely to be greater than 1.6 M_J. We demonstrate that the DoAr 44 disk's structure with a bright ring offset within a fainter skirt can be formed by dust particles drifting through a plausible distribution of gas.

24. The IGRINS YSO Survey III: Stellar parameters of pre-main sequence stars in Ophiuchus and Upper Scorpius

Ricardo López-Valdivia, Gregory N. Mace, Eunkyu Han, Erica Sawczynec, Jesús Hernández, L. Prato, Christopher M. Johns-Krull, Heeyoung Oh, Jae-Joon Lee, Adam Kraus, Joe Llama, Daniel T. Jaffe ★ We used the Immersion GRating Infrared Spectrometer (IGRINS) to determine fundamental parameters for 61 K- and M-type young stellar objects (YSOs) located in the Ophiuchus and Upper Scorpius star-forming regions. We employed synthetic spectra and a Markov chain Monte Carlo approach to fit specific K-band spectral regions and determine the photospheric temperature ($T_{\rm eff}$), surface gravity (log g), magnetic field strength (B), projected rotational velocity ($v \sin i$), and K-band veiling ($r_{\rm K}$). We determined B for $\sim$46the results from Taurus-Auriga and the TW Hydrae Association (TWA) presented in Paper I of this series. We classified all the YSOs in the IGRINS survey with infrared spectral indices from 2MASS and WISE photometry between 2 and 24 μm. We found that Class II YSOs typically have lower log g and $v \sin i$, similar B, and higher K-band veiling than their Class III counterparts. Additionally, we determined the stellar parameters for a sample of K and M field stars also observed with IGRINS. We have identified intrinsic similarities and differences at different evolutionary stages with our homogeneous determination of stellar parameters in the IGRINS YSO Survey. Considering log g as a proxy for age, we found that the Ophiuchus and Taurus samples have a similar age. We also find that Upper Scorpius and TWA YSOs have similar ages, and are more evolved than Ophiuchus/Taurus YSOs.

25. Mapping Protoplanetary Disk Vertical Structure with CO Isotopologue Line Emission

Charles J. Law, Richard Teague, Karin I. Öberg, Evan A. Rich, Sean M. Andrews, Jaehan Bae, Myriam Benisty, Stefano Facchini, Kevin Flaherty, Andrea Isella, Sheng Jin, Jun Hashimoto, Jane Huang, Ryan A. Loomis, Feng Long, Carlos E. Muñoz-Romero, Teresa Paneque-Carreño, Laura M. Pérez, Chunhua Qi, Kamber R. Schwarz, Jochen Stadler, Takashi Tsukagoshi, David J. Wilner, Gerrit van der Plas ★ High spatial resolution observations of CO isotopologue line emission in protoplanetary disks at mid-inclinations (≈30-75 degrees) allow us to characterize the gas structure in detail, including radial and vertical substructures, emission surface heights and their dependencies on source characteristics, and disk temperature profiles. By combining observations of a suite of CO isotopologues, we can map the 2D (r, z) disk structure from the disk upper atmosphere, as traced by CO, to near the midplane, as probed by less abundant isotopologues. Here, we present high angular resolution ($\lesssim$0."1 to ≈0."2; ≈15-30 au) observations of CO, ^{13}CO, and C^{18}O in either or both J=2-1 and J=3-2 lines in the transition disks around DM Tau, Sz 91, LkCa 15, and HD 34282. We derived line emission surfaces in CO for all disks and in ^{13}CO for the DM Tau and LkCa 15 disks. With these observations, we do not resolve the vertical structure of C^{18}O in any disk, which is instead consistent with C^{18}O emission originating from the midplane. Both the J=2-1 and J=3-2 lines show similar heights. Using the derived emission surfaces, we computed radial and vertical gas temperature distributions for each disk, including empirical temperature models for the DM Tau and LkCa 15 disks. After combining our sample with literature sources, we find that ^{13}CO line emitting heights are also tentatively linked with source characteristics, e.g., stellar host mass, gas temperature, disk size, and show steeper trends than seen in CO emission surfaces.

26. First detection of CHD_2OH towards pre-stellar cores

Yuxin Lin, Silvia Spezzano, Paola Caselli ★ The inheritance of material across the star and planet formation process is traced by deuterium fractionation. We report here the first detection of doubly deuterated methanol towards pre-stellar cores. We study the deuterium fractionation of methanol, CH_3OH, towards two starless and two pre-stellar cores. We derive a D/H ratio of 0.8-1.9% with CH_2DOH in pre-stellar cores H-MM1 and L694-2, consistent with measurements in more evolved Class 0/I objects and comet 67P/Churyumov-Gerasimenko, suggesting a direct chemical link arising in the pre-stellar stage. Furthermore, the column density ratios of CHD_2OH/CH_2DOH are ∼50-80%, consistently high as that towards Class 0/I objects, indicating an efficient formation mechanism of CHD_2OH, possibly through H atom additions to D_2CO. The CH_2DOH/CH_3OH and CHD_2OH/CH_3OH column density ratios in the two pre-stellar cores are larger than that in the two starless cores B68 and L1521E, representing an evolutionary trend of methanol deuteration in early-stage cores.

27. Rossby numbers of fully and partially convective stars

N. R. Landin, L. T. S. Mendes, L. P. R. Vaz, S. H. P. Alencar ★ We investigate stellar magnetic activity from the theoretical point of view, by using stellar evolution models to calculate theoretical convective turnover times (τ_c) and Rossby numbers (Ro) for pre-main-sequence and main-sequence stars. The problem is that the canonical place where τ_c is usually determined (half a mixing length above the base of the convective zone) fails for fully convective stars and there is no agreement on this in the literature. Our calculations were performed with the ATON stellar evolution code. We concentrated our analysis on fully and partially convective stars motivated by recent observations of slowly rotating fully convective stars, whose X-ray emissions correlate with their Rossby numbers in the same way as in solar-like stars, suggesting that the presence of a tachocline is not required for magnetic field generation. We investigate the behaviour of τ_c over the stellar radius for stars of different masses and ages. As Ro depends on τ_c, which varies strongly with the stellar radius, we use our theoretical results to determine a better radial position at which to calculate it for fully convective stars. Using our alternative locations, we fit a sample of 847 stars in the rotation-activity diagram (L_X/L_{bol} versus Ro) with a two-part power-law function. Our fit parameters are consistent with previous work, showing that stars with Ro$\leq$Ro$_{sat}$ are distributed around a saturation level in L_X/L_{bol} and, for stars with Ro>$\mathrm{Ro_{sat}}$, L_X/L_{bol} clearly decays with Ro with an exponent of -2.4 ± 0.1.

28. The role of the turbulence driving mode for the Initial Mass Function

Sajay Sunny Mathew, Christoph Federrath, Amit Seta ★ Turbulence is a critical ingredient for star formation, yet its role for the initial mass function (IMF) is not fully understood. Here we perform magnetohydrodynamical (MHD) simulations of star cluster formation including gravity, turbulence, magnetic fields, stellar heating and outflow feedback to study the influence of the mode of turbulence driving on IMF. We find that simulations that employ purely compressive turbulence driving (COMP) produce a higher fraction of low-mass stars as compared to simulations that use purely solenoidal driving (SOL). The characteristic (median) mass of the sink particle (protostellar) distribution for COMP is shifted to lower masses by a factor of 1.5 compared to SOL. Our simulation IMFs capture the important features of the observed IMF form. We find that turbulence-regulated theories of the IMF match our simulation IMFs reasonably well in the high-mass and low-mass range, but underestimate the number of very low-mass stars, which form towards the later stages of our simulations and stop accreting due to dynamical interactions. Our simulations show that for both COMP and SOL, the multiplicity fraction is an increasing function of the primary mass, although the multiplicity fraction in COMP is higher than that of SOL for any primary mass range. We find that binary mass ratio distribution is independent of the turbulence driving mode. The average specific angular momentum of the sink particles in SOL is a factor of 2 higher than that for COMP. Overall, we conclude that the turbulence driving mode plays a significant role in shaping the IMF.

29. An expanding ring of the hypercompact HII region W49N:A2

Ryosuke Miyawaki, Masahiko Hayashi, Tetsuo Hasegawa ★ We present 250 GHz continuum and H29alpha line data toward W49N:A2, a hypercompact HII region ionized by an O9 star. The data obtained with ALMA at a resolution of 0"05 (600 au) confirmed the presence of an ionized ring with a radius of 700 au inclined by 50degree (0degree for pole-on). It has a width of 1000 au and is relatively flat with a scale height of less than several hundred au. The tilted ring, or the apparent ellipse, has a prominent velocity difference between its NW and SE ridges along the minor axis, suggesting that it is expanding in the equatorial plane at a velocity of 13.2 km/s. The ring also shows a hint of rotation at 2.7 km/s, which is significantly (2.5sigma) smaller than the Kepler velocity of 5.2 km/s at its radius around the 20 $M_\odot$ star. This can be interpreted that the ring gas has been transported from the radius of 170 au by conserving its original specific angular momentum that it had there. The ionized ring may thus be a remnant of the accretion disk that fed the O9 star, whose radiation or magnetic activities became so strong that the disk accretion was reversed due to the intense thermal or magneto-hydrodynamic pressure around the star. The data has revealed a rare example of how a massive star terminates its accretion at the end of its formation, transforming a hypercompact HII region into an ultracompact HII region.

30. Evolution of the Angular Momentum of Molecular Cloud Cores Formed from Filament Fragmentation

Yoshiaki Misugi, Shu-ichiro Inutsuka, Doris Arzoumanian ★ The angular momentum of molecular cloud cores plays an essential role in the star formation process. However, the time evolution of the angular momentum of molecular cloud cores is still unclear. In this paper, we perform three-dimensional simulations to investigate the time evolution of the angular momentum of molecular cloud cores formed through filament fragmentation. As a result, we find that most of the cores rotate perpendicular to the filament axis. The mean angular momentum of the cores changes by only around 30the initial stage of their formation process and then remains almost constant. In addition, we analyze the internal angular momentum structure of the cores. Although the cores gain angular momentum with various directions from the initial turbulent velocity fluctuations of their parent filaments, the angular momentum profile in each core converges to the self-similar solution. We also show that the degree of complexity of the angular momentum structure in a core slightly decreases with time. Moreover, we perform synthetic observations and show that the angular momentum profile measured from the synthetic mean velocity map is compatible with the observations when the filament inclination is taken into account. The present study suggests a theory of core formation from filament fragmentation where the angular momentum structures of the cores are determined by the velocity fluctuation along the filaments and both are compatible with the observations. This theory also provides new insights on the core properties that could be observationally tested.

31. Impact of HAC evolution on the formation of small hydrocarbons in the Orion Bar and the Horsehead PDRs

M. S. Murga, A. I. Vasyunin, M. S. Kirsanova ★ We study evolution of hydrogenated amorphous carbon (HAC) grains under harsh UV radiation in photo-dissociation regions (PDRs) near young massive stars. Our aim is to evaluate the impact of the HAC grains on formation of observed small hydrocarbons: C_2H, C_2H_2, C_3H^+, C_3H, C_3H_2, C_4H, in PDRs. We developed a microscopic model of the HAC grains based on available experimental results. The model includes processes of photo- and thermodesorption, accretion of hydrogen and carbon atoms and subsequent formation of carbonaceous mantle on dust surface. H_2, CH_4, C_2H_2, C_2H_4, C_2H_6, C_3H_4, C_3H_6, C_3H_8 are considered as the main fragments of the HAC photo-destruction. We simulated evolution of the HAC grains under the physical conditions of two PDRs, the Orion Bar and the Horsehead nebula. We estimated the production rates of the HAC fragments in gas phase chemical reactions and compared them with the production rates of fragments due to the HAC destruction. The latter rates may dominate under some conditions, namely, at A_V=0.1 in both PDRs. We coupled our model with the gas-grain chemical model MONACO and calculated abundances of observed small hydrocarbons. We conclude that the contribution of the HAC destruction fragments to chemistry is not enough to match the observed abundances, although it increases the abundances by several orders of magnitude in the Orion Bar at A_V=0.1. Additionally, we found that the process of carbonaceous mantle formation on dust surface can be an inhibitor for the formation of observed small hydrocarbons in PDRs.

32. Cold Deuterium Fractionation in the Nearest Planet-Forming Disk

Carlos E. Muñoz-Romero, Karin I. Öberg, Charles J. Law, Richard Teague, Yuri Aikawa, Jennifer B. Bergner, David J. Wilner Jane Huang, Viviana V. Guzmán, L. Ilsedore Cleeves ★ Deuterium fractionation provides a window to the thermal history of volatiles in the solar system and protoplanetary disks. While evidence of active molecular deuteration has been observed towards a handful of disks, it remains unclear whether this chemistry affects the composition of forming planetesimals due to limited observational constraints on the radial and vertical distribution of deuterated molecules. To shed light on this question, we introduce new ALMA observations of DCO^+ and DCN $J = 2 - 1$ at an angular resolution of 0.5" (30 au) and combine them with archival data of higher energy transitions towards the protoplanetary disk around TW Hya. We carry out a radial excitation analysis assuming both LTE and non-LTE to localize the physical conditions traced by DCO^+ and DCN emission in the disk, thus assessing deuterium fractionation efficiencies and pathways at different disk locations. We find similar disk-averaged column densities of 1.9×10^{12} and 9.8×10^{11} cm^{-2} for DCO^+ and DCN, with typical kinetic temperatures for both molecules of 20-30K, indicating a common origin near the comet- and planet-forming midplane. The observed DCO^+/DCN abundance ratio, combined with recent modeling results, provide tentative evidence of a gas phase C/O enhancement within < 40 au. Observations of DCO^+ and DCN in other disks, as well as HCN and HCO^+, will be necessary to place the trends exhibited by TW Hya in context, and fully constrain the main deuteration mechanisms in disks.

33. Dust hot spots at 10 au scales around the Class 0 binary IRAS 16293-2422 A: a departure from the passive irradiation model

M. J. Maureira, M. Gong, J. E. Pineda, H. B. Liu, K. Silsbee, P. Caselli, J. Zamponi, D. Segura-Cox, A. Schmiedeke ★ Characterizing the physical conditions at disk scales in Class 0 sources is crucial for constraining the protostellar accretion process and the initial conditions for planet formation. We use ALMA 1.3 mm and 3 mm observations to investigate the physical conditions of the dust around the Class 0 binary IRAS 16293-2422 A (sep <100 au) down to 10 au scales. The circumbinary material's spectral index, alpha, has a median of 3.1 and a dispersion of 0.2, providing no firm evidence of mm-sizes grains therein. Continuum substructures with brightness temperature peaks of T_b 60-80 K at 1.3 mm are observed near the disks at both wavelengths. These peaks do not overlap with strong variations of alpha, indicating they trace high-temperature spots instead of regions with significant optical depth variations. The lower limits to the inferred dust temperature in the hot spots are 122, 87 and 49 K. Depending on the assumed dust opacity index, these values can be several times higher. They overlap with high gas temperatures and enhanced complex organic molecular (COM) emission. This newly resolved dust temperature distribution is in better agreement with the expectations from mechanical instead of the most commonly assumed radiative heating. In particular, we find that the temperatures agree with shock heating predictions. This evidence and recent studies highlighting accretion heating in Class 0 disks suggest that mechanical heating (shocks, dissipation powered by accretion, etc.) is important during the early stages and should be considered when modeling and measuring properties of deeply embedded protostars and disks.

34. Gas accretion onto Jupiter mass planets in discs with laminar accretion flows

R. P. Nelson, E. Lega, A. Morbidelli ★ (Abridged) Studies have shown that a Jovian mass planet embedded in a viscous protoplanetary disc (PPD) can accrete gas efficiently through the gap and doubles its mass in ~ 0.1 Myr. The planet also migrates inwards on a timescale of ~ 0.1 Myr. These timescales are short compared to PPD lifetimes, and raise questions about the origins of cold giant exoplanets. However, PPDs are unlikely to be globally turbulent, and instead they may launch magnetised winds such that accretion towards the star occurs in laminar accretion flows located in narrow layers near the surfaces of the disc. The aim of this study is to examine the rate at which gas accretes onto Jovian mass planets that are embedded in layered PPDs. We use 3D hydrodynamical simulations of planets embedded in PPDs, in which a constant radial mass flux towards the star of $\dot{m} = 10^{-8}$ M$_\odot$ yr^{-1} is sustained. We consider a classical viscous alpha model, and also models in which an external torque is applied in narrow surface layers to mimic the effects of a magnetised wind. The accreting layers are parameterised by their column densities $\Sigma_{\rm A}$, and we consider values in the range 0.1 to 10 g cm^{-2}. The viscous model gives results in agreement with previous studies. We find the accretion rate onto the planet in the layered models crucially depends on the planet's ability to block the wind-induced mass flow. For $\Sigma_{\rm A} = 10$ g cm^{-2}, the planet torque can block the mass flow through the disc, accretion onto the planet is slow, and a mass doubling time of 10 Myr is obtained. For $\Sigma_{\rm A} = 0.1$ g cm^{-2}, accretion is fast and the mass doubling time is 0.2 Myr. Although the radial mass flow through the layered disc models is always 10^{-8} M$_\odot$ yr^{-1}, adopting different values of $\Sigma_{\rm A}$ leads to very different gas accretion rates onto gas giant planets.

35. Environmental Effects of Star-Forming Cores on Mass Accretion Rate

Shingo Nozaki, Masahiro N. Machida ★ We calculate the evolution of cloud cores embedded in different envelopes to investigate environmental effects on the mass accretion rate onto protostars. As the initial state, we neglect the magnetic field and cloud rotation, and adopt star-forming cores composed of two parts: a centrally condensed core and an outer envelope. The inner core has a critical Bonnor-Ebert density profile and is enclosed by the outer envelope. We prepare 15 star-forming cores with different outer envelope densities and gravitational radii, within which the gas flows into the collapsing core, and calculate their evolution until $\sim 2 \times 10^5$ yr after protostar formation. The mass accretion rate decreases as the core is depleted when the outer envelope density is low. In contrast, the mass accretion rate is temporarily enhanced when the outer envelope density is high and the resultant protostellar mass exceeds the initial mass of the centrally condensed core. Some recent observations indicate that the mass of prestellar cores is too small to reproduce the stellar mass distribution. Our simulations show that the mass inflow from outside the core contributes greatly to protostellar mass growth when the core is embedded in a high-density envelope, which could explain the recent observations.

36. The evolution of circumstellar discs in the Galactic Centre: an application to the G-clouds

James E. Owen, Douglas N. C. Lin ★ The Galactic Centre is known to have undergone a recent star formation episode a few Myrs ago, which likely produced many T Tauri stars hosting circumstellar discs. It has been suggested that these discs may be the compact and dusty ionized sources identified as "G-clouds". Given the Galactic Centre's hostile environment, we study the possible evolutionary pathways these discs experience. We compute new external photoevaporation models applicable to discs in the Galactic Centre that account for the sub-sonic launching of the wind and absorption of UV photons by dust. Using evolutionary disc calculations, we find that photoevaporation's rapid truncation of the disc causes them to accrete onto the central star rapidly. Ultimately, an accreting circumstellar disc has a lifetime $\lesssim 1$ Myr, which would fail to live long enough to explain the G-clouds. However, we identify a new evolutionary pathway for circumstellar discs in the Galactic Centre. Removal of disc material by photoevaporation prevents the young star from spinning down due to magnetic braking, ultimately causing the rapidly spinning young star to torque the disc into a "decretion disc" state which prevents accretion. At the same time, any planetary companion in the disc will trap dust outside its orbit, shutting down photoevaporation. The disc can survive for up to $\sim$10 Myr in this state. Encounters with other stars are likely to remove the planet on Myr timescales, causing photoevaporation to restart, giving rise to a G-cloud signature. A giant planet fraction of $\sim 10\%$ can explain the number of observed G-clouds.

37. Near-infrared spectroscopy of a massive young stellar object in the direction toward the Galactic Center: XCN and aromatic C-D features

Takashi Onaka, Itsuki Sakon, Takashi Shimonishi ★ We report near-infrared (2.5–5 micron) long-slit (30 arcsec) spectroscopy of a young stellar object in the direction toward the Galactic center with the Infrared Camera on board the AKARI satellite. The present target is suggested to be AFGL 2006 based on its very red color and close location. The spectra show strong absorption features of H_2O and CO_2 ices, and emission of HI Br alpha recombination line and the 3.3 micron band, the latter of which originates from polycyclic aromatic hydrocarbons (PAHs) or materials containing PAHs. The spectra show a broad, complex absorption feature at 4.65 micron, which is well explained by a combination of absorption features of CO ice, CO gas, and XCN, and HI Pf beta emission. The spectra also indicate excess emission at 4.4 micron. The characteristics of the spectra suggest that the object is a massive young stellar object. The XCN feature shows a good correlation with the Br alpha emission, suggesting that the photolysis by ultraviolet photons plays an important role in the formation of the XCN carriers, part of which are attributed to OCN^-. The 4.4 micron emission shows a good correlation with the 3.3 micron PAH emission, providing supporting evidence that it comes from the aromatic C-D stretching vibration. The formation of OCN^- is of importance for the formation process of prebiotic matter in the interstellar medium (ISM), while the detection of aromatic C-D emission provides valuable information on the deuteration process of PAHs in the ISM and implications on the hiding site of the missing deuterium in the ISM.

38. ALMA-IMF VII – Investigating the origin of stellar masses: CMF evolution in the W43-MM2&MM3 mini-starburst

Y. Pouteau, F. Motte, T. Nony, M. Gonzalez, I. Joncour, J. -F. Robitaille, G. Busquet, R. Galvan-Madrid, A. Gusdorf, P. Hennebelle, A. Ginsburg, T. Csengeri, P. Sanhueza, P. Dell'Ova, A. M. Stutz, A. P. M. Towner, N. Cunningham, F. Louvet, A. Men'shchikov, M. Fernandez-Lopez, N. Schneider, M. Armante, J. Bally, T. Baug, M. Bonfand, S. Bontemps, L. Bronfman, N. Brouillet, D. Diaz-Gonzalez, F. Herpin, B. Lefloch, H. -L. Liu, X. Lu, F. Nakamura, Q. Nguyen Luong, F. Olguin, K. Tatematsu, M. Valeille-Manet ★ Among the most central open questions on the initial mass function (IMF) of stars is the impact of the environment on the shape of the core mass function (CMF) and thus potentially on the IMF. The ALMA-IMF Large Program aims to investigate the variations of the core distributions with cloud characteristics, as diagnostic observables of the formation process and evolution. The present study focuses on the W43-MM2&MM3 mini-starburst, whose CMF has been recently found to be top-heavy with respect to the Salpeter slope. W43-MM2&MM3 is a useful test case for environmental studies because it harbors a rich cluster containing a statistically significant number of cores, previously characterized in paper III. We applied a multiscale decomposition technique on the ALMA 1.3 mm and 3 mm continuum images to define six subregions. For each subregion we characterize the high column density probability distribution function, n-PDF, shape of the cloud gas using the 1.3 mm image. Using the core catalog, we investigate correlations between the CMF, n-PDF and core mass segregation. We classify the subregions into different stages of evolution, from quiescent to burst to post-burst, based on the surface number density of cores, number of outflows, and UCHii presence. The high-mass end of the subregion CMFs vary from being close to the Salpeter slope (quiescent) to top-heavy (burst and post-burst). Moreover, the second tail of the n-PDF varies from steep, to flat like observed for the high mass star-forming clouds. We found that subregions with flat second n-PDF tails display top-heavy CMFs. The CMF may evolve from Salpeter to top-heavy throughout the star formation process from the quiescent to the burst phase. This scenario raises the question of if the CMF might revert again to Salpeter as the cloud approaches the end of its star formation stage, a hypothesis that remains to be tested.

39. Star formation timescale in the molecular filament WB 673

O. L. Ryabukhina, M. S. Kirsanova, C. Henkel, D. S. Wiebe ★ We present observations of ammonia emission lines toward the interstellar filament WB 673 hosting the dense clumps WB 673, WB 668, S233-IR and G173.57+2.43. LTE analysis of the lines allows us to estimate gas kinetic temperature ($\lesssim 30$ K in all the clumps), number density ($7-17\times10^3$ cm^{-3}), and ammonia column density ($\approx 1-1.5\times10^{15}$ cm^{-2}) in the dense clumps. We find signatures of collapse in WB 673 and presence of compact spatially unresolved dense clumps in S233-IR. We reconstruct 1D density and temperature distributions in the clumps and estimate their ages using astrochemical modelling. Considering CO, CS, NH_3 and N_2H^+ molecules (plus HCN and HNC for WB 673), we find a chemical age of $t_{\rm chem} = 1-3\times10^5$ yrs providing the best agreement between the simulated and observed column densities in all the clumps. Therefore, we consider $t_{\rm chem}$ as the chemical age of the entire filament. A long preceding low-density stage of gas accumulation in the astrochemical model would break the agreement between the simulated and observed column densities. We suggest that rapid star formation over a $\sim 10^5$ yrs timescale take place in the filament.

40. Significance Mode Analysis (SigMA) for hierarchical structures. An application to the Sco-Cen OB association

Sebastian Ratzenböck, Josefa E. Großschedl, Torsten Möller, João Alves, Immanuel Bomze, Stefan Meingast ★ We present a new clustering method, Significance Mode Analysis (SigMA), to extract co-spatial and co-moving stellar populations from large-scale surveys such as ESA Gaia. The method studies the topological properties of the density field in the multidimensional phase space. We validate SigMA on simulated clusters and find that it outperforms competing methods, especially in cases where many clusters are closely spaced. We apply the new method to Gaia DR3 data of the closest OB association to Earth, Scorpio-Centaurus (Sco-Cen), and find more than 13,000 co-moving young objects, with about 19% of these having a sub-stellar mass. SigMA finds 37 co-moving clusters in Sco-Cen. These clusters are independently validated by their narrow HRD sequences and, to a certain extent, by their association with massive stars too bright for Gaia, hence unknown to SigMA. We compare our results with similar recent work and find that the SigMA algorithm recovers richer populations, is able to distinguish clusters with velocity differences down to about 0.5 km s^{-1}, and reaches cluster volume densities as low as 0.01 sources/pc^3. The 3D distribution of these 37 coeval clusters implies a larger extent and volume for the Sco-Cen OB association than typically assumed in the literature. Additionally, we find the association to be more actively star-forming and dynamically more complex than previously thought. We confirm that the star-forming molecular clouds in the Sco-Cen region, namely, Ophiuchus, L134/L183, Pipe Nebula, Corona Australis, Lupus, and Chamaeleon, are part of the Sco-Cen The application of SigMA to Sco-Cen demonstrates that advanced machine learning tools applied to the superb Gaia data allows to construct an accurate census of the young populations, to quantify their dynamics, and to reconstruct the recent star formation history of the local Milky Way.

41. Determining Dust Properties in Protoplanetary Disks: SED-derived Masses and Settling With ALMA

Anneliese Rilinger, Catherine Espaillat, Zihua Xin, Álvaro Ribas, Enrique Macías, Sarah Luettgen ★ We present spectral energy distribution (SED) modeling of 338 disks around T Tauri stars from eleven star-forming regions, ranging from ~0.5 to 10 Myr old. The disk masses we infer from our SED models are typically greater than those reported from (sub)mm surveys by a factor of 1.5-5, with the discrepancy being generally higher for the more massive disks. Masses derived from (sub)mm fluxes rely on the assumption that the disks are optically thin at all millimeter wavelengths, which may cause the disk masses to be underestimated since the observed flux is not sensitive to the whole mass in the disk; SED models do not make this assumption and thus yield higher masses. Disks with more absorbing material should be optically thicker at a given wavelength; which could lead to a larger discrepancy for disks around massive stars when the disk temperature is scaled by the stellar luminosity. We also compare the disk masses and degree of dust settling across the different star-forming regions and find that disks in younger regions have more massive disks than disks in older regions, but a similar degree of dust settling. Together, these results offer potential partial solutions to the "missing" mass problem: disks around T Tauri stars may indeed have enough material to form planetary systems, though previous studies have underestimated the mass by assuming the disks to be optically thin; these planetary systems may also form earlier than previously theorized since significant dust evolution (i.e., settling) is already apparent in young disks.

42. Modelling the CO streamers in the explosive ejection of Orion BN/KL region

Ary Rodríguez-González, Pedro Ruben Rivera-Ortiz, Antonio Castellanos-Ramírez, Alejandro C. Raga, Liliana Hernández-Martínez, Jorge Cantó, Luis A. Zapata, Fátima Robles-Valdez ★ We present reactive gasdynamic, axisymmetric simulations of dense, high velocity clumps for modelling the CO streamers observed in Orion BN/KL. We have considered 15 chemical species, a cooling function for atomic and molecular gas, and heating through cosmic rays. Our numerical simulations explore different ejection velocities, interstellar medium density configurations, and CO content. Using the CO density and temperature, we have calculated the CO ($J = 2 \rightarrow 1$) emissivity, and have built CO maps and spatially resolved line profiles, allowing us to see the CO emitting regions of the streamers and to obtain position velocity diagrams to compare with observations. We find that in order to reproduce the images and line profiles of the BN/KL CO streamers and H_2 fingers, we need to have clumps that first travel within a dense cloud core, and then emerge into a lower-density environment.

43. Building the molecular cloud population: the role of cloud mergers

Maya S. Skarbinski, Sarah M. R. Jeffreson, Alyssa A. Goodman ★ We study the physical drivers of slow molecular cloud mergers within a simulation of a Milky Way-like galaxy in the moving-mesh code Arepo, and determine the influence of these mergers on the mass distribution and star formation efficiency of the galactic cloud population. We find that 83 per cent of these mergers occur at a relative velocity below 5 km/s, and are associated with large-scale atomic gas flows, driven primarily by (1) expanding bubbles of hot, ionised gas caused by supernova explosions and (2) galactic rotation. The major effect of these mergers is to aggregate molecular mass into higher-mass clouds: mergers account for over 50 per cent of the molecular mass contained in clouds of mass M $> 2 \times 10^6$ Msun. These high-mass clouds have higher densities, internal velocity dispersions and instantaneous star formation efficiencies than their unmerged, lower-mass precursors. As such, the mean instantaneous star formation efficiency in our simulated galaxy, with its merger rate of just 1 per cent of clouds per Myr, is 25 per cent higher than in a similar population of clouds containing no mergers.

44. Measuring the 8621 Å Diffuse Interstellar Band in Gaia DR3 RVS Spectra: Obtaining a Clean Catalog by Marginalizing over Stellar Types

Andrew K. Saydjari, Catherine Zucker, J. E. G. Peek, Douglas P. Finkbeiner ★ Diffuse interstellar bands (DIBs) are broad absorption features associated with interstellar dust and can serve as chemical and kinematic tracers. Conventional measurements of DIBs in stellar spectra are complicated by residuals between observations and best-fit stellar models. To overcome this, we simultaneously model the spectrum as a combination of stellar, dust, and residual components, with full posteriors on the joint distribution of the components. This decomposition is obtained by modeling each component as a draw from a high-dimensional Gaussian distribution in the data-space (the observed spectrum) – a method we call "Marginalized Analytic Data-space Gaussian Inference for Component Separation" (MADGICS). We use a data-driven prior for the stellar component, which avoids missing stellar features not included in synthetic line lists. This technique provides statistically rigorous uncertainties and detection thresholds, which are required to work in the low signal-to-noise regime that is commonplace for dusty lines of sight. We reprocess all public Gaia DR3 RVS spectra and present an improved 8621 Å DIB catalog, free of detectable stellar line contamination. We constrain the rest-frame wavelength to 8623.14 ± 0.087 Å (vacuum), find no significant evidence for DIBs in the Local Bubble from the $1/6^{\mathrm{th}}$ of RVS spectra that are public, and show unprecedented correlation with kinematic substructure in Galactic CO maps. We validate the catalog, its reported uncertainties, and biases using synthetic injection tests. We believe MADGICS provides a viable path forward for large-scale spectral line measurements in the presence of complex spectral contamination.

45. Heavy-element Accretion by Proto-Jupiter in a Massive Planetesimal Disk, Revisited

Sho Shibata, Ravit Helled, Hiroshi Kobayashi ★ Planetesimal accretion is a key source for heavy-element enrichment in giant planets. It has been suggested that Jupiter's enriched envelope is a result of planetesimal accretion during its growth assuming it formed in a massive planetesimal disk. In this study, we simulate Jupiter's formation in this scenario. We assume in-situ formation and perform N-body simulations to infer the solid accretion rate. We find that tens-Earth masses of planetesimals can be captured by proto-Jupiter during the rapid gas accretion phase. However, if several embryos are formed near Jupiter's core, which is an expected outcome in the case of a massive planetesimal disk, scattering from the embryos increases the eccentricity and inclination of planetesimals and therefore significantly reduces the accretion efficiency. We also compare our results with published semi-analytical models and show that these models cannot reproduce the N-body simulations especially when the planetesimal disk has a large eccentricity and inclination. We show that when the dynamical evolution of planetesimals is carefully modelled, the total mass of captured planetesimals $M_{\mathrm{cap,tot}}$ is $2M_\oplus \lesssim M_{\mathrm{cap,tot}} \lesssim 18M_\oplus$. The metallicity of Jupiter's envelope can be explained by the planetesimal accretion in our massive disk model despite the low accretion efficiency coming from the high eccentricity and inclination of planetesimals. Our study demonstrates the importance of detailed modelling of planetesimal accretion during the planetary growth and its implications to the heavy-element mass in gaseous planets.

46. Comets and Planetesimal Formation

Jacob B. Simon, Jürgen Blum, Til Birnstiel, David Nesvorný ★ In this chapter, we review the processes involved in the formation of planetesimals and comets. We will start with a description of the physics of dust grain growth and how this is mediated by gas-dust interactions in planet-forming disks. We will then delve into the various models of planetesimal formation, describing how these planetesimals form as well as their resulting structure. In doing so, we focus on and compare two paradigms for planetesimal formation: the gravitational collapse of particle over-densities (which can be produced by a variety of mechanisms) and the growth of particles into planetesimals via collisional and gravitational coagulation. Finally, we compare the predictions from these models with data collected by the Rosetta and New Horizons missions and that obtained via observations of distant Kuiper Belt Objects.

47. Non-ideal magnetohydrodynamic simulations of the first star formation: the effect of ambipolar diffusion

Kenji Eric Sadanari, Kazuyuki Omukai, Kazuyuki Sugimura, Tomoaki Matsumoto, Kengo Tomida ★ In the present-day universe, magnetic fields play such essential roles in star formation as angular momentum transport and outflow driving, which control circumstellar disc formation/fragmentation and also the star formation efficiency. While only a much weaker field has been believed to exist in the early universe, recent theoretical studies find that strong fields can be generated by turbulent dynamo during the gravitational collapse. Here, we investigate the gravitational collapse of a cloud core ($\sim 10^3$ cm^{-3}) up to protostar formation ($\sim 10^{20}$ cm^{-3}) by non-ideal magnetohydrodynamics (MHD) simulations considering ambipolar diffusion (AD), the dominant non-ideal effects in the primordial-gas. We systematically study rotating cloud cores either with or without turbulence and permeated with uniform fields of different strengths. We find that AD can slightly suppress the field growth by dynamo especially on scales smaller than the Jeans-scale at the density range $10^{10} - 10^{14}$ cm^{-3}, while we could not see the AD effect on the temperature evolution, since the AD heating rate is always smaller than compression heating. The inefficiency of AD makes the field as strong as $10^3 - 10^5$ G near the formed protostar, much stronger than in the present-day cases, even in cases with initially weak fields. The magnetic field affects the inflow motion when amplified to the equipartition level with turbulence on the Jeans-scale, although disturbed fields do not launch winds. This might suggest that dynamo amplified fields have smaller impact on the dynamics in the later accretion phase than other processes such as ionisation feedback.

48. Using Molecular Gas Observations to Guide Initial Conditions for Star Cluster Simulations

Alison Sills, Steven Rieder, Anne S. M. Buckner, Alvaro Hacar, Simon Portegies Zwart, Paula S. Teixeira ★ The earliest evolution of star clusters involves a phase of co-existence of both newly-formed stars, and the gas from which they are forming. Observations of the gas in such regions provide a wealth of data that can inform the simulations which are needed to follow the evolution of such objects forward in time. We present a method for transforming the observed gas properties into initial conditions for simulations that include gas, stars, and ongoing star formation. We demonstrate our technique using the Orion Nebula Cluster. Since the observations cannot provide all the necessary information for our simulations, we make choices for the missing data and assess the impact of those choices. We find that the results are insensitive to the adopted choices of the gas velocity in the plane of the sky. The properties of the surrounding gas cloud (e.g. overall density and size), however, have an effect on the star formation rate and pace of assembly of the resultant star cluster. We also analyze the stellar properties of the cluster and find that the stars become more tightly clustered and in a stronger radial distribution even as new stars form in the filament.

49. A Census of the Low Accretors. II: Accretion Properties

Thanawuth Thanathibodee, Brandon Molina, Javier Serna, Nuria Calvet, Jesús Hernández, James Muzerolle, Ramiro Franco-Hernández ★ Much is known about the processes driving accretion from protoplanetary disks onto low-mass pre-main-sequence stars (T Tauri stars). Nevertheless, it is unclear how accretion stops. To determine the accretion properties and their relation to stellar properties and gain insight into the last stages of accretion, we present a detailed analysis of 24 low and possible accretors, previously identified using the He I $\lambda10830$ line. We model moderate-resolution Hα profiles of these stars using magnetospheric accretion flow models that account for the chromospheric contribution at the line center. Based on parameters derived from the fits of 20 stars that can be reproduced with the models, we find a power-law relation between the disk truncation radius and the mass accretion rate consistent with predictions from theory and simulations. Comparing the corotation and truncation radii, we find that most of our targets are accreting in the unstable regime and rule out the propeller as the main process stopping accretion. For the truncation radius to be the same as the magnetic radius, the dipole magnetic field and/or the efficiency parameter ξ need to be smaller than previously determined, suggesting that higher-order fields dominate in low accretion rates. Lastly, we determine that the lowest accretion rates that can be detected by Hα line modeling are $1-3\times10^{-11}M_{\odot}yr^{-1}$ for M3 stars and $3-5\times10^{-11}M_{\odot}yr^{-1}$ for K5 stars. These limits are lower than the observed accretion rates in our sample, suggesting that we have reached a physical lower limit. This limit, $\dot{M}\sim10^{-10}M_{\odot}yr^{-1}$, is consistent with EUV-dominated photoevaporation.

50. JCMT BISTRO Observations: Magnetic Field Morphology of Bubbles Associated with NGC 6334

Mehrnoosh Tahani and the Bistro team ★ We study the HII regions associated with the NGC 6334 molecular cloud observed in the sub-millimeter and taken as part of the B-fields In STar-forming Region Observations (BISTRO) Survey. In particular, we investigate the polarization patterns and magnetic field morphologies associated with these HII regions. Through polarization pattern and pressure calculation analyses, several of these bubbles indicate that the gas and magnetic field lines have been pushed away from the bubble, toward an almost tangential (to the bubble) magnetic field morphology. In the densest part of NGC 6334, where the magnetic field morphology is similar to an hourglass, the polarization observations do not exhibit observable impact from HII regions. We detect two nested radial polarization patterns in a bubble to the south of NGC 6334 that correspond to the previously observed bipolar structure in this bubble. Finally, using the results of this study, we present steps (incorporating computer vision; circular Hough Transform) that can be used in future studies to identify bubbles that have physically impacted magnetic field lines.

51. Modeling the CO outflow in DG Tau B: Swept-up shells versus perturbed MHD disk wind

A. de Valon, C. Dougados, S. Cabrit, F. Louvet, L. A. Zapata, D. Mardones ★ The origin of outflows and their exact impact on disk evolution and planet formation remain crucial open questions. DG Tau B is a Class I protostar associated with a rotating conical CO outflow and a structured disk. Hence it is an ideal target to study these questions. We aim to characterize the morphology and kinematics of the DG Tau B outflow in order to elucidate its origin and potential impact on the disk. Our analysis is based on Atacama Large Millimeter Array (ALMA) 12CO(2-1) observations of DG Tau B at 20 au angular resolution. We characterize three different types of substructures in this outflow (arches, fingers, and cusps) with apparent acceleration. Wind-driven shell models with a Hubble law fail to explain these substructures. In contrast, both the morphology and kinematics of the conical flow can be explained by a steady conical magnetohydrodynamic (MHD) disk wind with foot-point radii r0= 0.7-3.4 au, a small magnetic level arm parameter lambda $<$ 1.6), and quasi periodic brightness enhancements. These might be caused by the impact of jet bow shocks, source orbital motion caused by a 25 MJ companion at 50 au, or disk density perturbations accreting through the wind launching region. The large CO wind mass flux (four times the accretion rate onto the central star) can also be explained if the MHD disk wind removes most of the angular momentum required for steady disk accretion. Our results provide the strongest evidence so far for the presence of massive MHD disk winds in Class I sources with residual infall, and they suggest that the initial stages of planet formation take place in a highly dynamic environment.

52. Formation of pebbles in (gravito-)viscous protoplanetary disks with various turbulent strengths

Eduard I. Vorobyov, Vardan G. Elbakyan, Anders Johansen, Michiel Lambrechts, Aleksandr M. Skliarevskii, O. P. Stoyanovskaya ★ Aims. Dust plays a crucial role in the evolution of protoplanetary disks. We study the dynamics and growth of initially sub-μm dust particles in self-gravitating young protoplanetary disks with various strengths of turbulent viscosity. We aim to understand the physical conditions that determine the formation and spatial distribution of pebbles when both disk self-gravity and turbulent viscosity can be concurrently at work. Methods. We perform the thin-disk hydrodynamics simulations of self-gravitating protoplanetary disks over an initial time period of 0.5 Myr using the FEOSAD code. Turbulent viscosity is parameterized in terms of the spatially and temporally constant α-parameter, while the effects of gravitational instability on dust growth is accounted for by calculating the effective parameter α_{GI}. We consider the evolution of dust component including momentum exchange with gas, dust self-gravity, and also a simplified model of dust growth. Results. We find that the level of turbulent viscosity strongly affects the spatial distribution and total mass of pebbles in the disk. The $\alpha = 10^{-2}$ model is viscosity-dominated, pebbles are completely absent, and dust-to-gas mass ratio deviates from the reference 1:100 value no more than by 30% throughout the disk extent. On the contrary, the $\alpha = 10^{-3}$ model and, especially, the $\alpha = 10^{-4}$ model are dominated by gravitational instability. The effective parameter $\alpha + \alpha_{GI}$ is now a strongly varying function of radial distance. As a consequence, a bottle neck effect develops in the innermost disk regions, which makes gas and dust accumulate in a ring-like structure. Abridged.

53. TESS Hunt for Young and Maturing Exoplanets (THYME) IX: a 27 Myr extended population of Lower-Centaurus Crux with a transiting two-planet system

Mackenna L. Wood and the THYME team ★ We report the discovery and characterization of a nearby (85 pc), older (27 +/- 3 Myr), distributed stellar population near Lower-Centaurus-Crux (LCC), initially identified by searching for stars co-moving with a candidate transiting planet from TESS (HD 109833; TOI 1097). We determine the association membership using Gaia kinematics, color-magnitude information, and rotation periods of candidate members. We measure it's age using isochrones, gyrochronology, and Li depletion. While the association is near known populations of LCC, we find that it is older than any previously found LCC sub-group (10-16 Myr), and distinct in both position and velocity. In addition to the candidate planets around HD 109833 the association contains four directly-imaged planetary-mass companions around 3 stars, YSES-1, YSES-2, and HD 95086, all of which were previously assigned membership in the younger LCC. Using the Notch pipeline, we identify a second candidate transiting planet around HD 109833. We use a suite of ground-based follow-up observations to validate the two transit signals as planetary in nature. HD 109833 b and c join the small but growing population of <100 Myr transiting planets from TESS. HD 109833 has a rotation period and Li abundance indicative of a young age (< 100 Myr), but a position and velocity on the outskirts of the new population, lower Li levels than similar members, and a CMD position below model predictions for 27 Myr. So, we cannot reject the possibility that HD 109833 is a young field star coincidentally nearby the population.

54. An ionized outflow in Orion-KL source I?

Melvyn Wright, Tomoya Hirota, Jan Forbrich, Richard Plambeck, John Bally, Ciriaco Goddi, Adam Ginsburg, Brett A. McGuire ★ We present images at 6 and 14 GHz of Source I in Orion-KL. At higher frequencies, from 43 to 340 GHz, images of this source are dominated by thermal emission from dust in a 100 AU diameter circumstellar disk, but at 6 and 14 GHz the emission is elongated along the minor axis of the disk, aligned with the SiO bipolar outflow from the central object. Gaussian fits to the 6, 14, 43, and 99 GHz images find a component along the disk minor axis whose flux and length vary with frequency consistent with free-free emission from an ionized outflow. The data favor a broad outflow from a disk wind, rather than a narrow ionized jet. Source I was undetected in higher resolution 5 GHz e-MERLIN observations obtained in 2021. The 5-6 GHz structure of SrcI may be resolved out by the high sidelobe structure of the e-MERLIN synthesized beam, or be time variable.

55. Measuring the Dust Masses of Protoplanetary Disks in Lupus with ALMA: Evidence that Disks can be Optically Thick at 3 mm

Z. Xin, C. C. Espaillat, A. M. Rilinger, A. Ribas, E. Macias ★ Accurate disk mass measurements are necessary to constrain disk evolution and the timescale of planet formation, but such measurements are difficult to make and are very dependent on assumptions. Here we look at the assumption that the disk is optically thin at radio wavelengths and the effect of this assumption on measurements of disk dust mass. We model the optical to radio spectral energy distributions (SEDs) of 41 protoplanetary disks located in the young (1-3 Myr old) Lupus star-forming region, including 0.89 mm, 1.33 mm, and 3 mm flux densities when available. We measure disk dust masses that are 1.5-6 times higher than when using the commonly adopted disk dust mass equation under the assumption of optically thin emission in the (sub-)millimeter. The cause of this discrepancy is that most disks are optically thick at millimeter wavelengths, even up to 3 mm, demonstrating that observations at longer wavelengths are needed to trace the fully optically thin emission of disks.

56. On the Spatial Distribution of ^{13}CO Structures within ^{12}CO Molecular Clouds

Lixia Yuan, Ji Yang, Fujun Du, Xunchuan Liu, Yang Su, Qing-Zeng Yan, Xuepeng Chen, Yan Sun, Shaobo Zhang, Xin Zhou, Yuehui Ma ★ We look into the 2851 ^{12}CO molecular clouds harboring ^{13}CO structures to reveal the distribution of the projected angular separations and radial velocity separations between their internal ^{13}CO structures. The projected angular separations are determined using the minimal spanning tree algorithm. We find that $\sim 50\%$ of the angular separations fall in a narrow range of $\sim 3-7$ arcmin with a median of ~ 5 arcmin, and the corresponding radial velocity separations mainly range from ~ 0.3 km s^{-1} to 2.5 km s^{-1}. The mean and standard deviation of the angular separations of the internal ^{13}CO structures within ^{12}CO clouds appear to be universal, independent of the ^{12}CO cloud angular areas and the counts of their internal ^{13}CO structures. We also reveal a scaling relation between the ^{12}CO cloud angular area and its harbored ^{13}CO structure count. These results suggest there is a preferred angular separation between ^{13}CO structures in these ^{12}CO clouds, considering the distance effects. According to that, we propose an alternative picture for the assembly and destruction of molecular clouds: there is a fundamental separation for the internal structures of molecular clouds, the build-up and destruction of molecular clouds proceeds under this fundamental unit.

57. Direct measurements of carbon and sulfur isotope ratios in the Milky Way

Y. T. Yan, C. Henkel, C. Kobayashi, K. M. Menten, Y. Gong, J. S. Zhang, H. Z. Yu, K. Yang, J. J. Xie, Y. X. Wang ★ With the IRAM 30 meter telescope, we performed observations of the $J = 2$-1 transitions of CS, C^{33}S, C^{34}S, C^{36}S, ^{13}CS, ^{13}C^{33}S, and ^{13}C^{34}S as well as the $J = 3$-2 transitions of C^{33}S, C^{34}S, C^{36}S, and ^{13}CS toward a large sample of 110 HMSFRs. We measured the ^{12}C/^{13}C, ^{32}S/^{34}S, ^{32}S/^{33}S, ^{32}S/^{36}S, ^{34}S/^{33}S, ^{34}S/^{36}S, and ^{33}S/^{36}S abundance ratios with rare isotopologs of CS, thus avoiding significant saturation effects. With accurate distances obtained from parallax data, we confirm previously identified ^{12}C/^{13}C and ^{32}S/^{34}S gradients as a function of galactocentric distance (RGC). In the CMZ, ^{12}C/^{13}C ratios are higher than suggested by a linear fit to the disk values as a function of RGC. While ^{32}S/^{34}S ratios near the Galactic center and in the inner disk are similar, this is not the case for ^{12}C/^{13}C, when comparing central values with those near RGC of 5 kpc. As was already known, there is no ^{34}S/^{33}S gradient but the average ratio of 4.35 ± 0.44 derived from the $J = 2$-1 transition lines of C^{34}S and C^{33}S is well below previously reported values. A comparison between solar and local interstellar ^{32}S/^{34}S and ^{34}S/^{33}S ratios suggests that the Solar System may have been formed from gas with a particularly high ^{34}S abundance. For the first time, we report positive gradients of ^{32}S/^{33}S, ^{34}S/^{36}S, ^{33}S/^{36}S, and ^{32}S/^{36}S in our Galaxy. The predicted ^{12}C/^{13}C ratios from the latest GCE models are in good agreement with our results. While ^{32}S/^{34}S and ^{32}S/^{36}S ratios show larger differences at larger RGC, ^{32}S/^{33}S ratios show an offset across the entire inner 12 kpc of the Milky Way.

58. The Solar Neighborhood in the Age of Gaia

Catherine Zucker, João Alves, Alyssa Goodman, Stefan Meingast, Phillip Galli ★ Most of what we know about the formation of stars, and essentially everything we know about the formation of planets, comes from observations of our solar neighborhood within 2 kpc of the Sun. Before 2018, accurate distance measurements needed to turn the 2D Sky into a faithful 3D physical picture of the distribution of stars, and the interstellar matter that forms them, were few and far between. Here, we offer a holistic review of how, since 2018, data from the Gaia mission are revealing previously unseen and often unexpected 3D distributions of gas, dust, and young stars in the solar neighborhood. We summarize how new extinction-based techniques yield 3D dust maps and how the density structure mapped out offers key context for measuring young stars' 3D positions from Gaia and VLBI. We discuss how a subset of young stars in Gaia with measured radial velocities and proper motions is being used to recover 3D cloud motion and characterize the internal dynamics of individual star-forming regions. We review relationships between newly-identified clusters and streams of young stars and the molecular interstellar medium from which they evolve. The combination of these measures of gas and stars' 3D distribution and 3D motions provides unprecedented data for comparison with simulations and reframes our understanding of local star formation in a larger Galactic context. This new 3D view of our solar neighborhood in the age of Gaia shows that star-forming regions once thought to be isolated are often connected on kiloparsec scales, causing us to reconsider models for the arrangement of gas and young stars in galaxies.

59. Supervised machine learning on Galactic filaments Revealing the filamentary structure of the Galactic interstellar medium

A. Zavagno, F. -X. Dupé, S. Bensaid, E. Schisano, G. Li Causi, M. Gray, S. Molinari, D. Elia, J. -C. Lambert, M. Brescia, D. Arzoumanian, D. Russeil, G. Riccio, S. Cavuoti ★ Context. Filaments are ubiquitous in the Galaxy, and they host star formation. Detecting them in a reliable way is therefore key towards our understanding of the star formation process. Aims. We explore whether supervised machine learning can identify filamentary structures on the whole Galactic plane. Methods. We used two versions of UNet-based networks for image segmentation.We used H2 column density images of the Galactic plane obtained with Herschel Hi-GAL data as input data. We trained the UNet-based networks with skeletons (spine plus branches) of filaments that were extracted from these images, together with background and missing data masks that we produced. We tested eight training scenarios to determine the best scenario for our astrophysical purpose of classifying pixels as filaments. Results. The training of the UNets allows us to create a new image of the Galactic plane by segmentation in which pixels belonging to filamentary structures are identified. With this new method, we classify more pixels (more by a factor of 2 to 7, depending on the classification threshold used) as belonging to filaments than the spine plus branches structures we used as input. New structures are revealed, which are mainly low-contrast filaments that were not detected before.We use standard metrics to evaluate the performances of the different training scenarios. This allows us to demonstrate the robustness of the method and to determine an optimal threshold value that maximizes the recovery of the input labelled pixel classification. Conclusions. This proof-of-concept study shows that supervised machine learning can reveal filamentary structures that are present throughout the Galactic plane. The detection of these structures, including low-density and low-contrast structures that have never been seen before, offers important perspectives for the study of these filaments.

60. Hydrodynamic turbulence in disks with embedded planets

Alexandros Ziampras, Wilhelm Kley, Richard P. Nelson ★ The vertical shear instability (VSI) is a source of hydrodynamic turbulence that can drive vigorous vertical mixing and moderate levels of accretion in protoplanetary disks, and it could be observable in the near future. With high-resolution three-dimensional numerical hydrodynamics simulations, we modeled the behavior of the VSI in protoplanetary disks with and without embedded planets. We then measured its accretion and mixing capabilities by comparing the full Reynolds stress, which includes the contribution of nonaxisymmetric features, such as spiral arms and vortices, to the Reynolds stress due to the azimuthally averaged velocity field, which can be attributed to good approximation to the VSI. We verified that the VSI can contribute to the accretion stress and showed that, depending on disk conditions, an embedded planet can coexist with or suppress VSI turbulent stress. Specifically, the presence of spiral shocks launched by a planet or planet-generated vortices can interfere with the VSI near the planet's vicinity, with the instability recovering at large enough distances from the planet or vortex. Our results suggest that observations of VSI signatures are unlikely in disks that contain massive, nonaxisymmetric features.